A Simplified Model for Excitability

AUTHOR(S):

Murase, Masatoshi

Lecture Note I (1992)
Graduate School of Science
Kyoto University

A Simplified Model for Excitability

Masatoshi Murase

Yukawa Institute for Theoretical Physics
Kyoto University

Our final goal is to develop a model for a flagellum which is considered to be a class of nonlinear distributed systems (see Seminar Note II). For this purpose, we need a simplified model for the local system. It is now established that muscle and flagella undergo the common molecular mechanism. In developing a theoretical model, therefore, we have to equally take into account experimental observations in muscle as well as in flagella. In the present paper, a simplified model is proposed based on the force-length relationship in the muscle system. Computer simulations and phase-plane methods reveal that the model exhibits complex bifurcation diagrams such as a *homoclinic* connection, a *Hopf* bifurcation and a *saddle-node* bifurcation. The onset and cessation of oscillations observed in the flagellar system are also interpreted in terms of the model behavior.

1. Introduction

Oscillations with high frequencies (~ 100 - 1000 Hz) —— sometimes these high-frequency oscillations are referred to as *hyperoscillations* —— have been observed in two different types of motile systems. One is the wingbeats of flying insects like mosquitoes. Each wingbeat results from a contraction of the insect flight muscle. The muscle contraction is in turn caused by a motor nerve impulse. Until 1949, it was believed that the origin of the rhythmic wingbeats was ascribed to the repetitive nerve impulses. However, Pringle [1] discovered that the motor nerve impulses were not always synchronized with wingbeats. His findings strongly suggest that the muscular oscillations are not caused by the repetitive firings of the motor neurons, but result from the intrinsic properties of the muscle itself. It has been a challenging problem in biophysics to clarify these intrinsic properties.

Another example of hyperoscillations is the vibrations of flagella. Generally, flagella show bending wave propagation with about 30-80 Hz. If such flagella are fragmented and placed between a glass slide

and a coverslip, these fragmented flagella do not beat, instead they display hyperoscillations [2]. As biochemical conditions are changed, these oscillations disappear. There are two ways by which oscillations disappear. In one, an inhibitor is added. This effect is interpreted as the decrease in the fraction of the active "cross-bridge", because it causes the decrease in the active force. The second way by which hyperoscillations disappear is through the reduction of the Mg-ATP concentration. As the Mg-ATP concentration is decreased, the vibration frequency decreases. The question now arising is how the motile systems exhibit the onset and cessation of oscillations.

In the present paper, a simplified model for excitability is proposed based on the force-length relationship in the muscle system. Then, the resultant model is used to explain the turning "on" and "off" of oscillations observed in the flagellar system. Using computer simulations and phase-plane methods, the bifurcation diagrams of this model are detailed.

2. The model

2.1. Mathematical description

The present model assumes that (i) a cross-bridge in the active state shows a cubic force-distance function, and (ii) there are passive elastic and external shear forces. Let x, n and Z be the dimensionless sliding displacement (x = 1 corresponds to 24 nm), the fraction of the active cross-bridges (varying continuously between 0 and 1), and the external shear force, respectively. Then, the model can be expressed as:

$$\gamma \frac{dx}{dt} = nf(x) - K_e x + Z \qquad (1a)$$

$$\frac{dn}{dt} = \begin{cases} b(1 - n) & (x \le x_a) \\ - cn & (x > x_a) \end{cases} \qquad (1b)$$

where

$$f(x) = Ax^2(1 - x)\,. \qquad (1c)$$

A, b, c, K_e, x_a and γ are the force constant of the active cross-bridges, the activation rate constant, the inactivation rate constant, the force constant of the passive elastic component, the activation region and the internal viscous shear resistance, respectively. Here b and c are in $msec^{-1}$, A, K_e and Z in pN per cross-bridge and γ in pNmsec per cross-bridge. Equation (1a) describes the balance of all the shear forces. Equation (1b) shows that n is allowed to change continuously between 0 (completely lacking in excitability) and 1 (maximal excitability), depending on x.

There are several ways by which dynamical properties of the model can be represented. One way to predict the model behavior is by numerical integration of equations (1). This numerical technique is useful in describing quantitatively the time evolution of state variables

x and n. In addition to using numerical techniques, it is also useful to deduce important qualitative properties of the solutions to equations (1) without explicitly solving it. Examples of such qualitative visualizations are the force-distance representation and the phase plane representation. The next three subsections describes these two qualitative analytical methods.

2.2. Force-distance relationship

By setting $dx/dt = 0$ in equation (1a), we have the following steady-state force-distance relationship for the model:

$$Z = - nf(x) + K_e x . \qquad (2)$$

Figure 1 illustrates such force-distance relationships in the (x, Z) plane. When n = 1, there is a cubic force-distance relationship which has three intersections, P_1, P_2 and P_3, with the x axis. These three points are the actual steady-state points when Z = 0. P_1 corresponds to a stable resting state, P_2 to an unstable threshold state, and P_3 to a stable excited state. Superthreshold x values lead to the excited state, P_3; while subthreshold x values lead to the resting state, P_1. This model, thus, accounts for a *threshold* phenomenon.

Instead of applying the superthreshold x values, an excited state is also achieved by increasing Z. As Z is increased (say, Z = 0.004), the intersections, P_1 and P_2, approach each other. A sufficiently large value for Z makes P_1 and P_2 disappear. As a result, the phase point moves toward P_3.

It is clear that the excited state is obtained by the shift of either x or Z. However, this excited state is not definitely stable because n begins to decrease according to equation (1b). We set $x_a = 0.2$, so that the excited state exists in the region where inactivation takes place (i.e. the decrease in n toward 0). The force-distance relationship changes dynamically from $Z = - f(x) + K_e x$ to $Z = K_e x$. The resultant force-distance relationship has only a single steady state at the origin, and so the system returns to this state. There is a refractory period during which the cubic force-distance relationship disappears, and hence there is no threshold phenomenon.

If Z is set at a value that causes the two intersections P_1 and P_2 vanish, the system no longer stays in a stable steady state, but instead displays oscillatory behaviors. Depending on the constant values of Z, a number of different rhythms arise in which low- and high-amplitude oscillations can be observed.

Now it should be noted that, if the external force, Z, the sliding displacement, x, and the fraction of the active cross-bridges, n, are viewed as the external current, I, the transmembrane voltage, V, and the generalized excitability parameter, Y (where Y can be considered as summing up the whole behavior of the *sodium activation* m, *sodium inactivation* h and *potassium activation* n of the Hodgkin-Huxley model [3]), then $Z = - f(x) + K_e x$ and $Z = K_e x$ are analogous to the current-voltage relationship for a maximally excitable membrane and that for a

completely inexcitable membrane. In this analogy, the model described by equations (1) accounts for the electrical excitability phenomena. Indeed this model resembles the simple version of the Hodgkin-Huxley model for an excitable membrane presented by van Capelle and Durrer [4] and extended by Landau et al. [5].

2.3 Phase-plane representation

The model behavior is completely described by the state variables x and n. Solutions to equations (1) can be represented as trajectories in the (x, n) phase plane. A typical trajectory is given in Figure 2, which corresponds to the solution in Figure 3. This figure also represents the *vertical isocline* or the *x-nullcline* (i.e. $\dot{x} = 0$) and the *horizontal isocline* or the *n-nullcline* ($\dot{n} = 0$). These nullclines are written as follows:

$$\dot{x} = 0 \qquad n = \frac{K_e x - Z}{A x^2 (1 - x)} \qquad (3a)$$

$$\dot{n} = 0 \qquad n = \begin{cases} 1 & (x \le x_a) \\ 0 & (x < x_a) \end{cases} \qquad (3b)$$

The intersections of the two nullclines give the steady-state points, P_1, P_2 and P_u. P_1 is a stable *node* (i.e. resting point), P_2 a *saddle* point (i.e. threshold point), and P_u an unstable point. Starting from the point (circled number 1), the phase point moves rapidly along a horizontal path. This part of the trajectory corresponds to the cross-bridge power stroke — or the upstroke of the "action-potential" like behavior — in Figure 3. This cross-bridge power stroke is followed by its inactivation leading to a decrease in n. As a result, the trajectory turns downward. When the phase point enters the local, activation region, it ascends vertically toward the resting point, P_1, resulting in the completion of the loop.

The last part of this trajectory determines the key features of the model behavior. The next section discusses how this part of the trajectory in the phase plane is influenced by the vector field and/or the shape of isoclines.

3. Excitability and oscillations in the motile system

3.1 Homoclinic orbit

Let us first consider the effect of a change in the vector field. For this purpose we shall change the value of activation rate b. For small values of b (say b = 1.3 as in Fig.2), the phase point moves toward the resting point, P_1. As b increases from 1.3, the trajectory in the region for $x \le x_a$ moves slightly upward (Figure 4 for b = 1.320), and at the critical value of b it touches the saddle point. This is known as *homoclinic orbit*. The homoclinic connection may be considered as a limit cycle of infinite period. As b continues to increase to b = 1.322, the phase point no longer moves toward the resting point, leaving a stable limit cycle oscillation with an amplitude of about 0.4 and a frequency of 133 Hz.

Although the vector field given by equations (1) varies continuously with b, there is a sudden appearance of a stable limit cycle across a threshold value of b. Figure 5 illustrates how a limit cycle appears as the parameter, b, is increased. When b = 1.3, a stable node, P_1, a saddle point, P_2, and an unstable fixed point, P_u coexist (left panel). The saddle point has a stable and an unstable *separatrix* as indicated by the arrowheads. As b is increased to the critical value (b = 1.321), the stable separatrix just touches the limit cycle, resulting in a homoclinic connection (middle panel). With further increases in b, the limit cycle oscillation spontaneously appears. As a result, there is a stable limit cycle, a stable node, and a saddle point in the phase plane (right panel). By reversing the parameter and decreasing b, the limit cycle suddenly disappears upon collision with the saddle point. After the annihilation of the limit cycle oscillation, there remains a saddle point and a stable node in the phase plane.

3.2 Dynamic hysteresis loop

It is also important to study the effect of changing the constant parameter, Z, on the *x*-nullcline. Figure 6A shows how the change in Z affects the shape of the *x*-nullcline, and hence the trajectories in the (*x*, n) phase plane. According to equation (3a), n is decreased by a positive change of Z for any x values. This change lowers the *x*-nullcline. Inversely, the *x*-nullcline is raised by a negative change of Z. The n-nullcline, however, is not modified by any of these changes.

Because of the short distance between the two intersections, P_1 and P_2, the locations of these intersections are very sensitive to small changes in the *x*-nullcline. As Z is increased from zero, the *x*-nullcline is lowered, so that P_1 moves to the right and P_2 to the left. As a result, P_1 and P_2 meet with each other, and then vanish (e.g. Z = 0.007). The resulting *x*-nullcline is characterized by an S-shaped sigmoid. As long as the S-shaped characteristic exists, oscillations of any amplitude and frequency appear. Figure 6B shows one example of such oscillations when Z = 0.02. The amplitude and frequency are about 0.3 (corresponding to about 7 nm) and 280 Hz, respectively. As Z continues to increase to Z = 0.04, the S-shaped characteristic is replaced by a rather monotonic curve. Oscillatory behavior ceased after oscillatory transients damped (Fig.6C). If Z is further increased to Z = 0.08, non-oscillatory decay of the motion appears (Fig.6D).

It is also interesting to note that the S-shaped *x*-nullcline in this model highly resembles nullclines of the biochemical models for excitability and oscillations [see e.g. 6], and those of the models for excitable membranes [see e.g. 4]. There appears to be common features for excitability and oscillations among quite diverse biochemical, electrophysiological, and mechano-chemical systems

Figure 7 depicts the bifurcation diagram as a function of Z. There are two types of dynamic hysteresis loops as labelled A and B. First consider the diagram labelled A. Starting in the oscillatory state (the upper solid curve) and decreasing Z, the limit cycle disappears through a homoclinic connection (see Fig.5) and the system jumps to a stable node (the lower solid curve). If Z is now increased, the stable

node will persist until it vanishes upon collision with a saddle (the middle broken curve). This is known as a saddle-node bifurcation or *fold* bifurcation. Figure 8A illustrates how a saddle-node bifurcation occurs. Through this saddle-node bifurcation, the limit cycle reappears.

Next consider the diagram labelled B. For small values of Z (< 0.03), there is a stable limit cycle (the lower solid curve). When Z is increased to Z > 0.03, there is also a stable steady state at $x = 0.2$ (the upper solid line), but the dynamics will be stuck at the stable limit cycle. However, as Z is further increased, the limit cycle disappears suddenly. If Z is now decreased, a stable steady state persists until Z < 0.03, and then a stable limit cycle oscillation of finite amplitude and frequency suddenly appears. This is known as a *subcritical* Hopf bifurcation or *hard excitation* as illustrated in Figure 8B. Unlike the general Hopf bifurcation, the dotted curve of the unstable limit cycle does not rise vertically from an unstable steady state when increasing Z. This occurs because the system lacks differentiability at $x = 0.2$ (see equation (1b).

The important characteristic common in both bifurcation diagrams (labelled A and B) is that for some ranges of parameter values there is *bi-stability* (i.e. a stable steady state coexists with a stable limit cycle). For a system possessing these types of characteristics, two interesting experiments are possible. In one, the system is subjected to an alternate increasing and decreasing control parameter. Either a stable steady state or a stable limit cycle might appear, depending on the history of the control parameter. Thus, the system dynamically switches oscillations "on" and "off". If the control parameter is increased and decreased slowly, compared with the frequency of the limit cycle oscillation, then the system can exhibit distinct burst-like activity.

In the second type of experiment, a brief stimulus of a certain strength is delivered at a critical phase of the ongoing limit cycle. It is possible that the system jumps to the stable state because of this stimulus, resulting in an abrupt loss of oscillation. Similarly, another stimulus can trigger oscillations when it is delivered to the quiescent system. The annihilation of oscillations induced by a single pulse-like perturbation has been discovered in cardiac pacemaker cells [7] and in nerve cells [8], but it has not yet been observed in flagellar systems.

4. Onset and cessation of hyperoscillations

Analysis in the previous section reveals that (i) oscillations of any amplitude and frequency can be present by modifying the vector field and/or nullclines; and (ii) the initiation and termination of limit cycle oscillations can be controlled by stimuli. Based on these considerations, we try to understand how hyperoscillations appear and disappear in the flagellar system.

As we have discussed, there are two ways by which hyperoscillations are annihilated: one is by the decrease in the frequency asymptotically toward 0, which is associated with a decrease in the ATP concentration; and the other is by the decrease in the

fraction of the cross-bridge in the force-generating state when an inhibitor is added.

Consider, for example, the stable limit cycle oscillation shown in Fig.6B. Figure 9 re-draws the same limit cycle trajectory (solid curve) as that in Fig.6B for b = 1.3 and Z = 0.02. We first consider the effects of lowering ATP concentration on hyperoscillations. For this purpose, we assume that the inactivation rate constant, c, is roughly proportional to the ATP concentration. As c decreases, the trajectory along which a phase point is moving is raised (dotted line) and the phase point stays longer on the x-nullcline. This means that the inactivation process becomes a rate limiting step, and hence the limit cycle oscillation slows down with the decrease of the frequency. When c = 0, the oscillation is completely annihilated. This model behavior corresponds to the experimental observation that hyperoscillations are annihilated through the decrease in the frequency when ATP concentration is lowered.

How can we interpret the effects of inhibitor in terms of the model behavior ? In order to account for these effects, equation (1b) should be rewritten as follows:

$$\frac{dn}{dt} = \begin{cases} b(n_0 - n) & (x \le x_a) \\ -cn & (x > x_a) \end{cases} \qquad (4)$$

where n_0 is the maximal fraction of cross-bridges in the force-generating state. Previously, we have assumed that $n_0 = 1$. However, it is reasonable to consider that n_0 is inversely proportional to the concentration of inhibitor. As n_0 is decreased from 1, the n-nullcline in the activation region ($x \le x_a$) is lowered as illustrated in Figure 10. There is no significant effect on the speed of motion of a phase point there, and so the frequency is not changed dramatically. At the critical value of n_0, a homoclinic connection appears. With a slight decrease in n_0, a limit cycle oscillation completely disappears in the phase plane. This model behavior, therefore, accounts for the cessation of hyperoscillations through the decrease in the fraction of cross-bridges in the active state when inhibitor is added.

5. Discussion

The theoretical model proposed here accounts for not only simple modes of excitability and oscillations, but also more complex bifurcation diagrams leading to bursting and chaos. Unfortunately, flagellar and ciliary dynamics have not been studied along this line, although some cilia actually show bursts of repeated cycles of beating [see 9]. One reason for this is that many cell biologists have been interested in the regular behaviors, such as the symmetric steady-state bend propagation typical of flagella and the asymmetric beat cycle with an effective and a recovery stroke typical of cilia, but not in the potential irregular behaviors. Although periodic perturbation methods have been applied to the flagellum [9,10], no one has ever investigated its aperiodic responsiveness. Another reason is that theoretical biologists have not tried to develop simple mathematical models in

this field, but instead have aimed to develop complicated models. They have been interested in qualitatively explaining specific modes of cilia and flagella. It is, therefore, very difficult to understand the essential features of the model.

I think that it is much better to have any "qualitative" agreement with experimental data than to make efforts to do "quantitative" curve fitting. So the point in this chapter is that (i) a very simple model can explain qualitative behaviors observed in experiments, and (ii) this model can potentially exhibit complex dynamics which may be observed in experiments in future.

References

[1] J. W. S. Pringle, J. Physiol. 108 (1949) 226.
[2] S. Kamimura and R. Kamiya, Nature 340 (1989) 476.
[3] A. L. Hodgkin and A. F. Huxley, J. Physiol. 117 (1952) 500.
[4] F. J. L. van Capelle and D. Durrer, Circ. Res. 47 (1980) 454.
[5] M. Landau, P. Lorente, J. Henry and S. Canu, J. Math. Biol. 25 (1987) 491.
[6] A. Goldbeter, Models for oscillations and excitability in biochemical systems, In Mathematical Models in Molecular and Cellular Biology, ed. L. A. Segel, Cambridge University Press, Cambridge (1980).
[7] J. Jalife and C. Antzelevitch, Science 206 (1979) 695.
[8] R. Guttman, S. Lewis and J. Rinzel, J. Physiol. 305 (1980) 377.
[9] M. A. Sleigh and D. I. Barlow, Symp. Soc. Exp. Biol. 35 (1982) 139.
[10] M. Okuno and Y. Hiramoto, J. Exp. Biol. 65 (1976) 401.
[11] I. R. Gibbons, C. Shingyoji, A. Murakami and K. Takahashi, Nature 325 (1987) 351.

Figure 1

Force-distance characteristics. The area denoted by a broken square in panel (A) is enlarged in panel (B). When Z = 0 and n = 1, there are three steady states with two stable states, P_1 and P_3, and one unstable state, P_2. As n decreases from 1 to 0, the cubic function is replaced by a monotonic function. Interestingly, these force-distance characteristics are analogous to the well known voltage-current characteristics of excitable membranes.

Figure 2

Phase plane of the model described by equations (1). One solution to this equation is represented by a trajectory marked with arrowheads. The circled numbers correspond to those in Figure 3. Three singular points, P_1, P_2, and P_u, occur at these intersections of x- and n-nullclines. P_1 is a stable node, P_2 a saddle point, and P_u an unstable point. The two intersections, P1 and P2, correspond to those in Fig.1. A threshold phenomenon appears at the saddle point. Parameters are: A = 6 pN, b = 1.3 $msec^{-1}$, c = 0.3 $msec^{-1}$, K_e = 0.4 pN, x_a = 0.2, γ = 0.1 pNmsec, and Z = 0. Initial conditions are: n = 1 and x = 0.1.

Figure 3

The time course of x and n. x shows an "action-potential" like behavior in nerve membrane. The circled numbers correspond to those in Fig.2. Prameters and initial conditions are as in Fig.2.

Figure 4

Influence of the parameter b. (A): For small parameter values (b = 1.320), the trajectory starts from the superthreshold initial conditions and returns to the stable point, P_1. This excitable behavior is similar to the previous case shown in Fig.2. When b is slightly larger (b = 1.322), there appears a closed trajectory on which a phase point circulates clockwise around the unstable point, P_u. This corresponds to a stable limit cycle oscillation with an amplitude of about 0.4 and a frequency of 133 Hz. (B): Enlarged detail of panel A to show two separating trajectories.

Figure 5

Sudden appearance of a limit cycle through a homoclinic connection. There is a stable node, P_1, a saddle point, P_2, and an unstable fixed point, P_u (left panel). As the parameter, b, is increased, the unstable separatrix of the saddle point meets with the stable separatrix, resulting in a homoclinic orbit (middle panel). The homoclinic orbit exists only for a single value of b. By increasing b, the limit cycle oscillation suddenly appears (right panel). Inversely, decreasing b makes the limit cycle disappear upon collision with the saddle point. This is the typical mechanism by which a limit cycle can abruptly vanish from a phase plane. The upper solid curve, middle broken line, and lower solid line represent the paths of the particular

phase point of the limit cycle, of the saddle point and of the stable node, respectively. If b is replaced by Z, this figure represents the emergence of the homoclinic orbit as observed in Fig.7.

Figure 6

Influence of the parameter, Z. The parameters and initial conditions are as in Figures 2 and 3, except for the value of Z. (A): When Z = 0, there are three intersections, P_1, P_2, and P_u, of the *x*- and n-nullclines. P_1 is a stable node, P_2 a saddle point, and P_u an unstable point. As Z is increased from 0, the *x*-nullcline is lowered without changing the n-nullcline. For Z = 0.007, the two intersections, P_1 and P_2, vanish upon collision, though there still remains an unstable point, P_u. However, if Z is further increased to Z = 0.03, the unstable point, P_u, disappears, and instead there appears a stable point, P_s. For Z > 0.03, there is always the stable point, P_s, as a single intersection of the two nullclines. (B): Limit cycle oscillation with an amplitude of about 0.3 and a frequency of 280 Hz for Z = 0.02. Starting from the initial conditions (i.e., n = 1 and x = 0.1), the trajectory converges on the stable limit cycle as shown by a solid curve with arrowheads. (C): Damped oscillation leading to a stable point, P_s, for Z = 0.04. The trajectory starts the same initial conditions. (D): Non-oscillatory decay of the model behavior for Z = 0.08.

Figure 7

Bifurcation diagram for the model described by equations (1) as a function of the control parameter, Z. The parameters are as in Figures 2, 3, and 6 except for the Z values. The upper broken line refers to an unstable fixed point. The lower broken curve refers to a saddle point. Besides them, there is a limit cycle, a stable node and a stable fixed point as indicated in the figure. The homoclinic connection in the broken rectangle labelled A resembles that in Fig.5. If b is viewed as Z, the same is true. The saddle-node bifurcation shown in the broken rectangle labelled A is detailed in Figure 8A. The Hopf bifurcation appears in the broken rectangle labelled B. This is detailed in Figure 8B.

Figure 8

(A): Saddle-node bifurcation. The bifurcation diagram shown in the broken rectangle A of Figure 7 is detailed. The upper broken and the lower solid curves correspond to the paths of the saddle point, P_1, and the stable node, P_2, respectively. As Z is increased, the two steady-state points approach each other (left panel), and then vanish (middle panel). As a result, every trajectory goes away to infinity (right panel). (B): Subcritical Hopf bifurcation (or Hard excitation). The bifurcation diagram shown in the broken rectangle B of Figure 7 is detailed. Initially, there is a stable limit cycle oscillation (solid trajectory) and an unstable fixed point, P_u, for a relatively small value of Z (left panel). As Z is increased, the unstable point, P_u, is converted to an unstable limit cycle (broken circle), leaving a stable fixed point, P_s

(middle panel). For a sufficiently large value of Z, the stable and unstable oscillations disappear and a single stable point remains (right panel). There is bistability (i.e. the stable point and stable limit cycle coexist) in the middle panel, so that hysteresis appears when the control parameter, Z, is increased and decreased.

Figure 9

Annihilation of oscillations accompanied by the decrease in their frequencies. The parameters are as in Figure 6B except for the values of c. When c = 0.3, there is the same trajectory as in Fig.6B. If c is decreased, the phase point moves slowly in the region of $x > x_a$ (see equation (1b)). As a result, the frequency of oscillation decreases. When c = 0, the trajectory approaches the stable point depending on the initial conditions. This means that oscillation is annihilated. This dynamical behavior probably accounts for the effects of the change in ATP concentration in the experiments by Kamimura and Kamiya [2].

Figure 10

Annihilation of oscillations due to the decrease in the fraction of the cross-bridge in the force generating state. The parameters are as in Figure 6B except for n_0. As n_0 is decreased from 1, the n-nullcline in the region for $x \leq x_a$ is lowered. When n_0 = 0.5, there is little difference in the trajectory, so that the frequency is not changed significantly. As n_0 is decreased, the homoclinic connection appears. For n_0 = 0.25, the phase point moves toward the stable fixed point. Thus, the oscillation is annihilated without changing its frequency. This behavior may account for the effects of vanadate in the experiments by Kamimura and Kamiya [2].

(A)

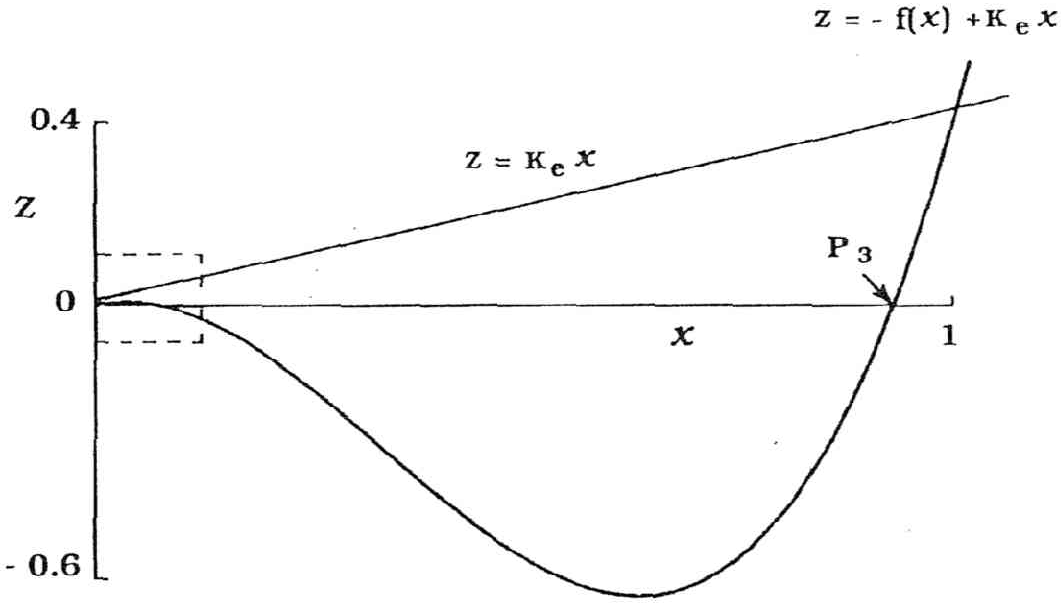

(B)

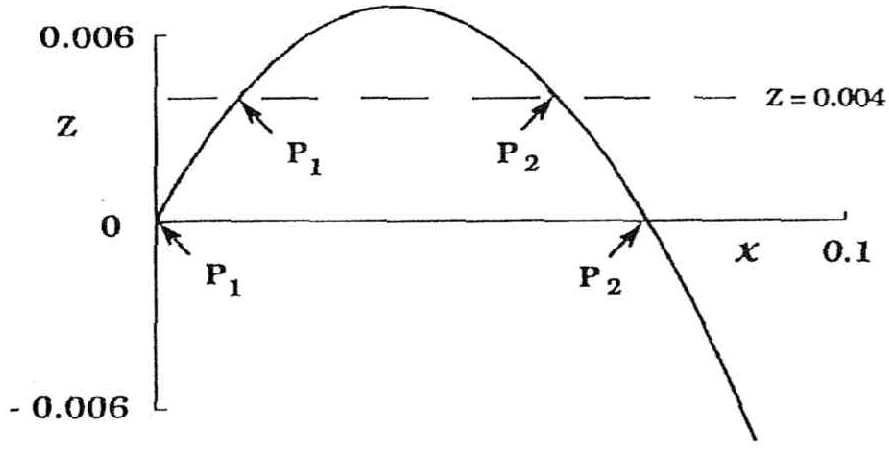

Fig. 1

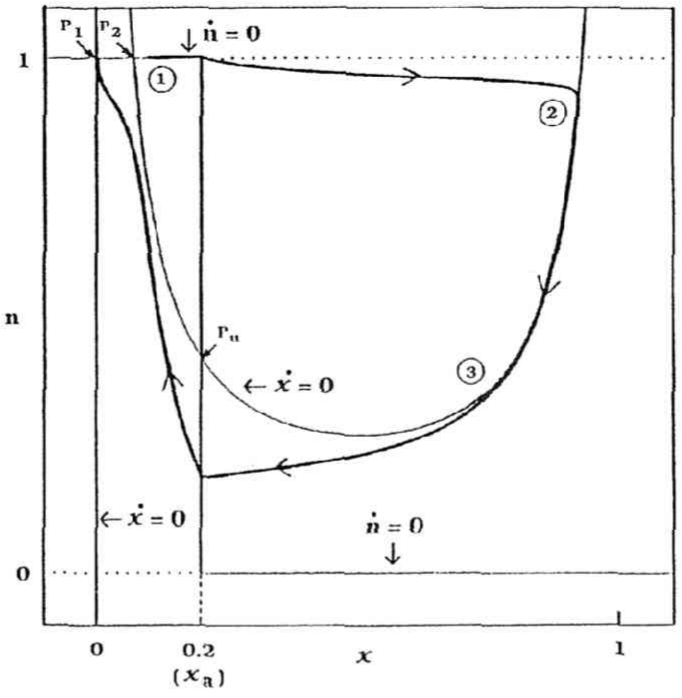

Fig.2

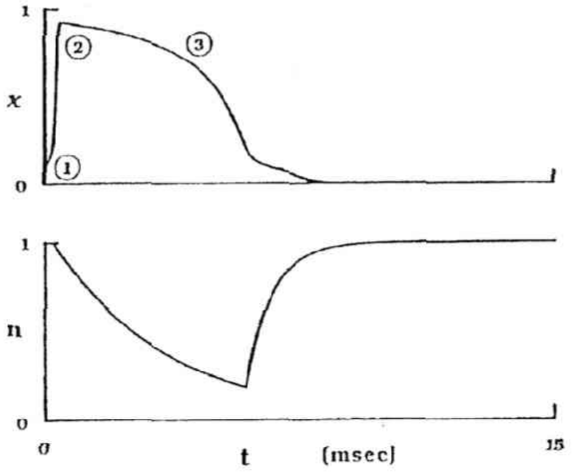

Fig.3

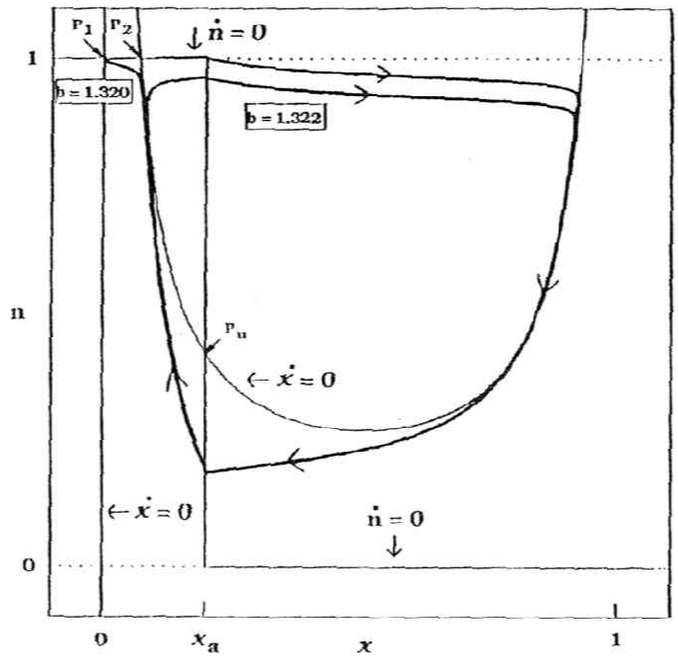

Fig.4A

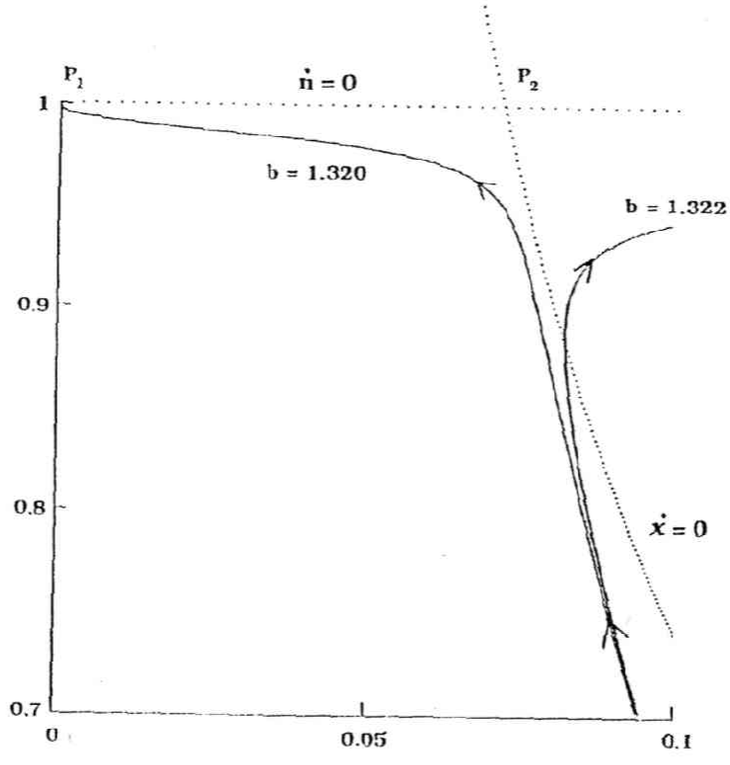

Fig.4B

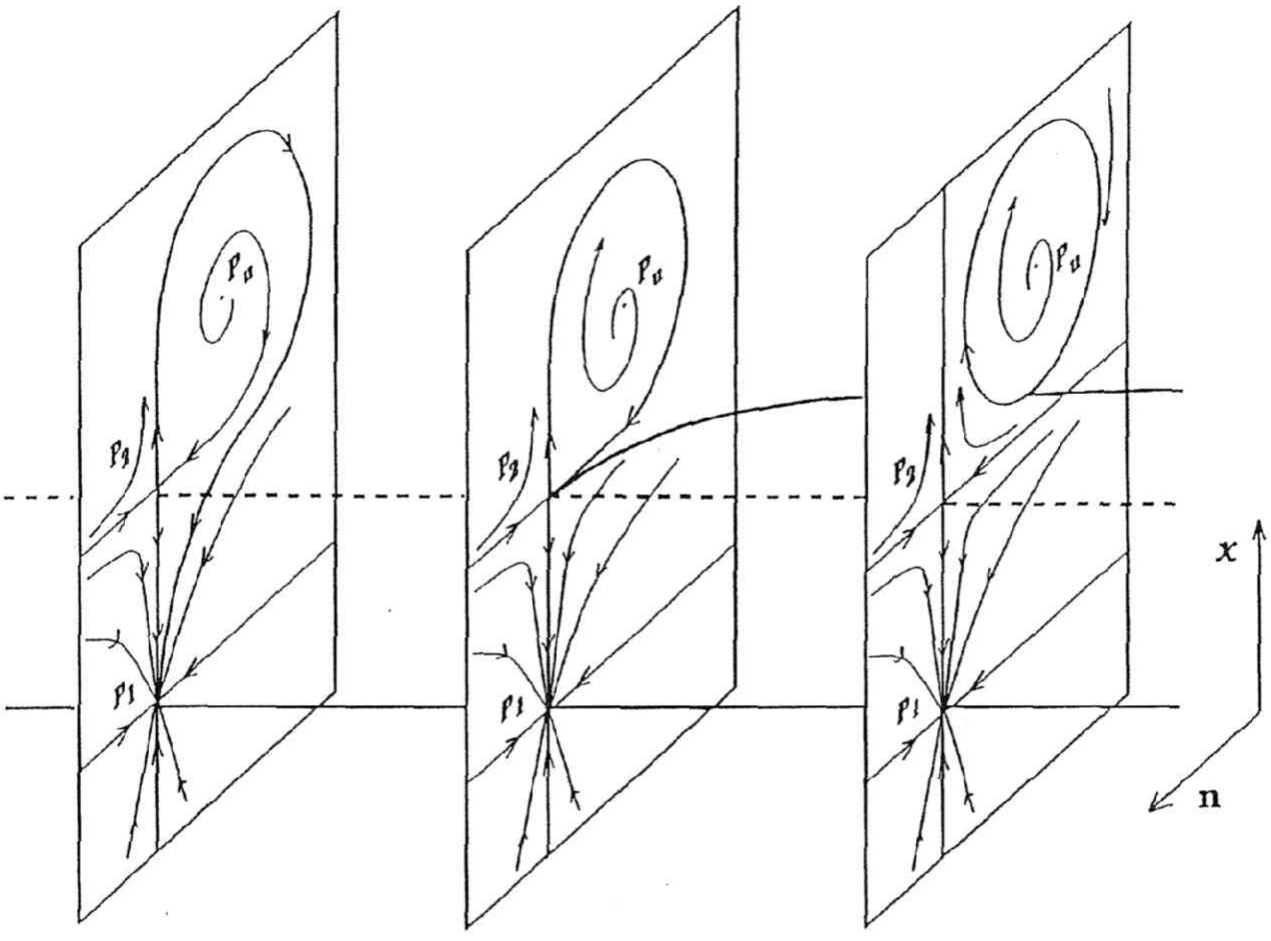

Fig.5

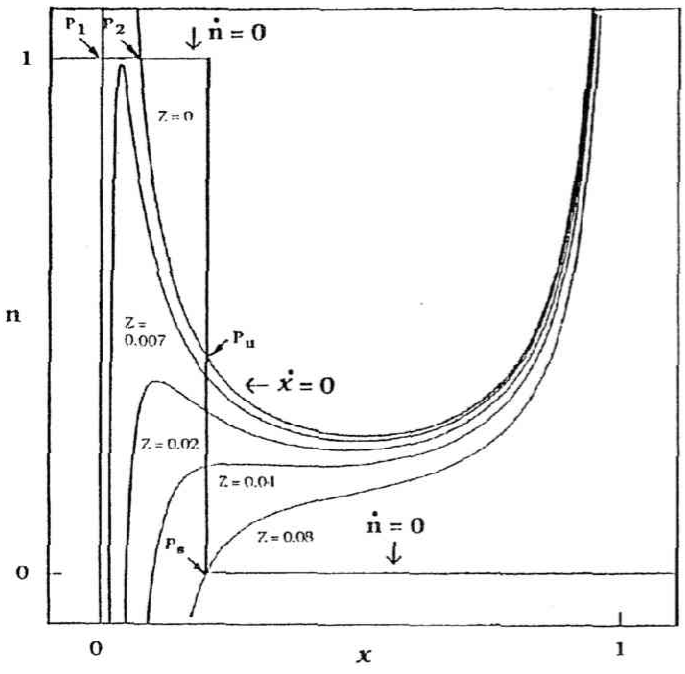

Fig.6A

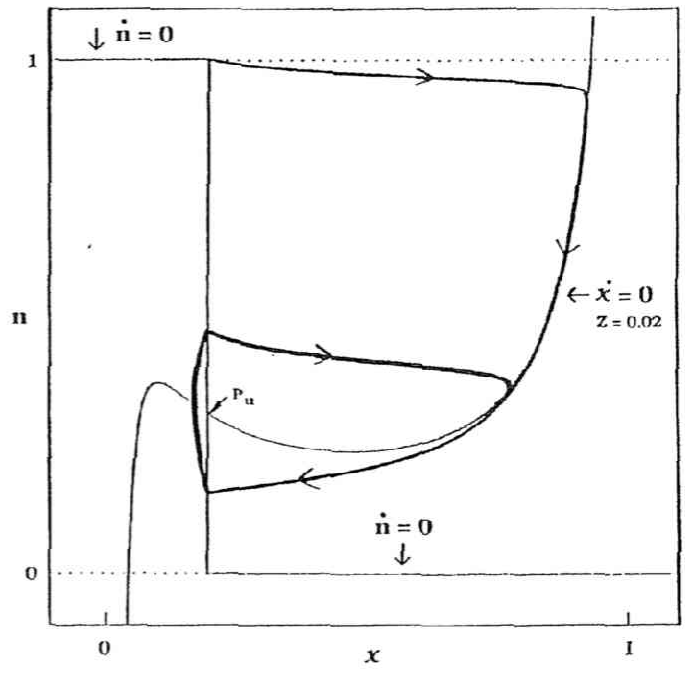

Fig.6B

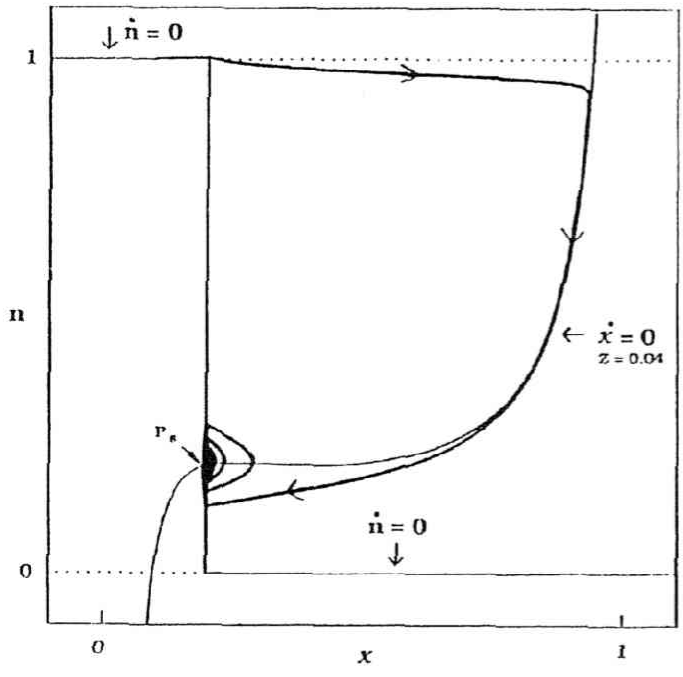

Fig.6C

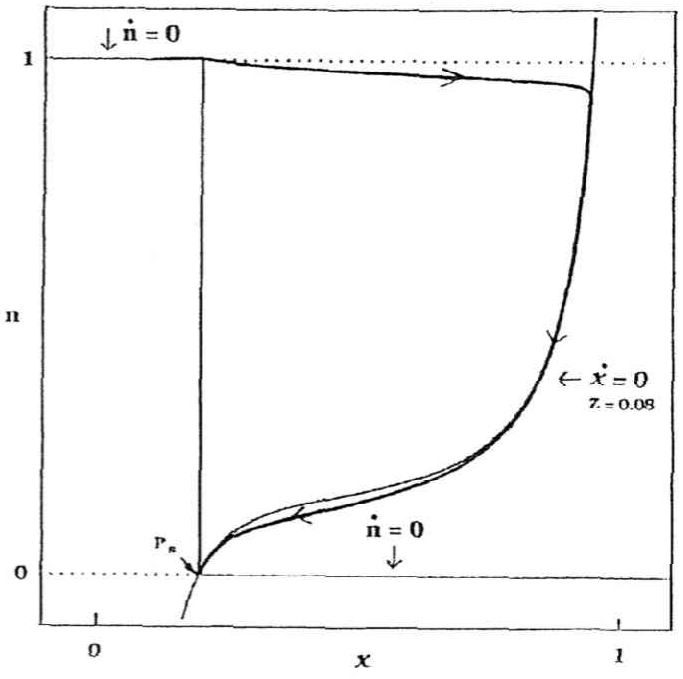

Fig.6D

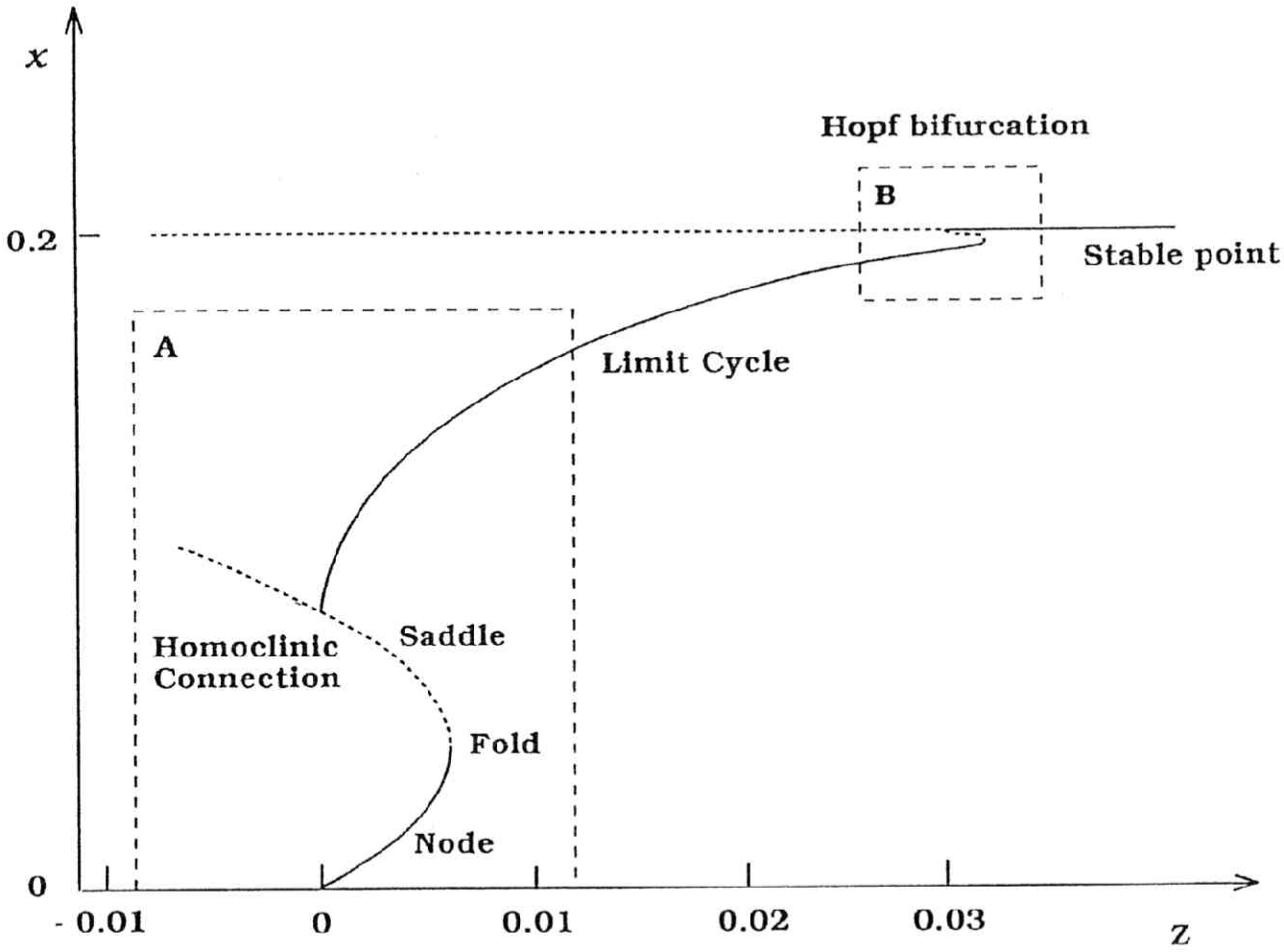

Fig.7

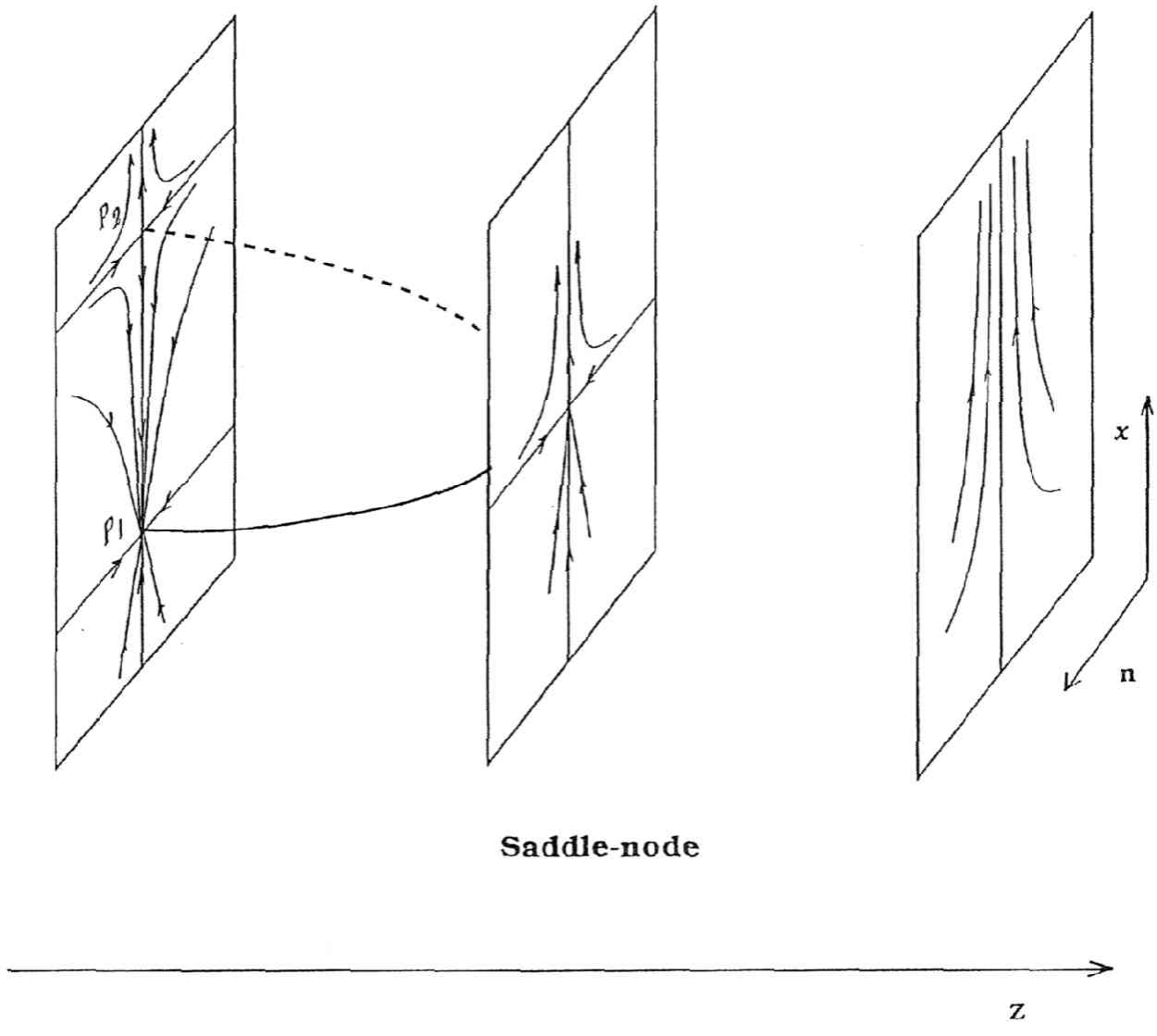

Fig.8A

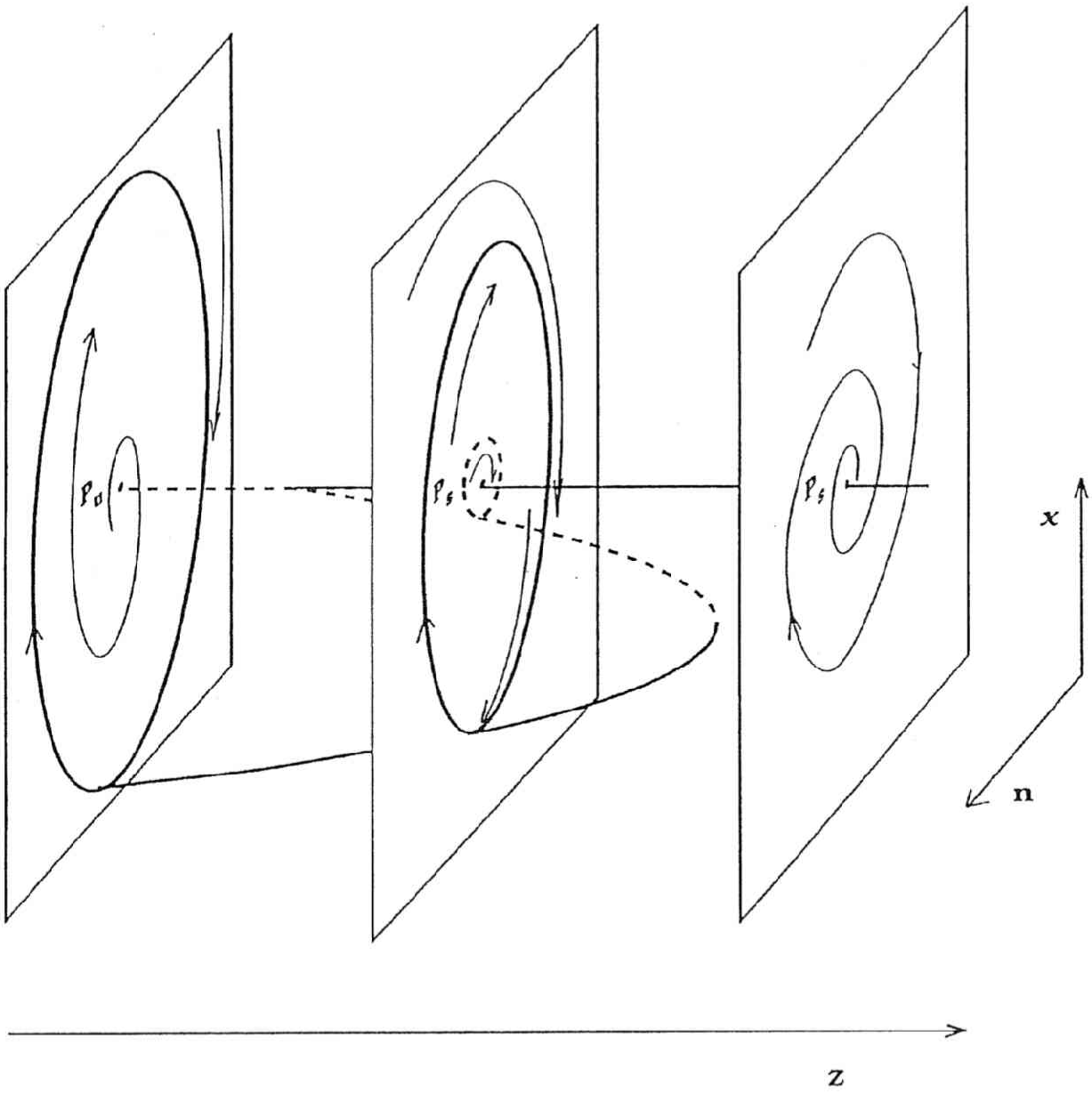

Fig.8B

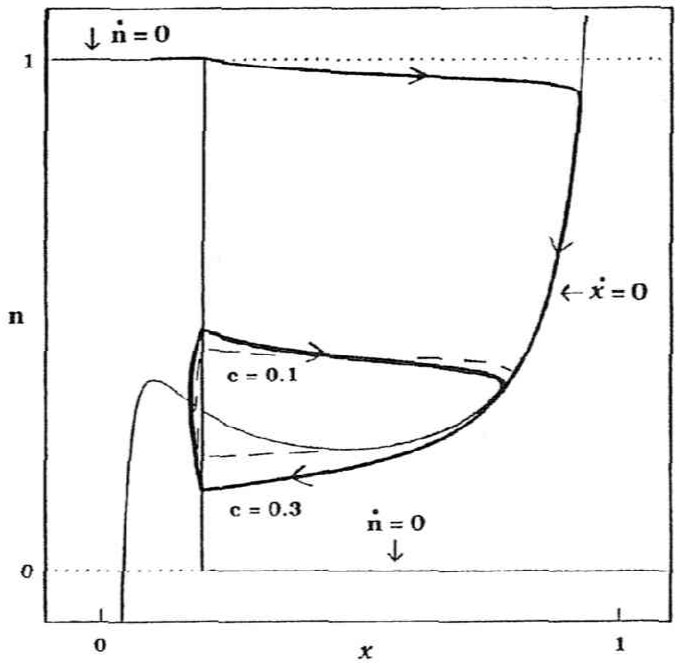

Fig.9

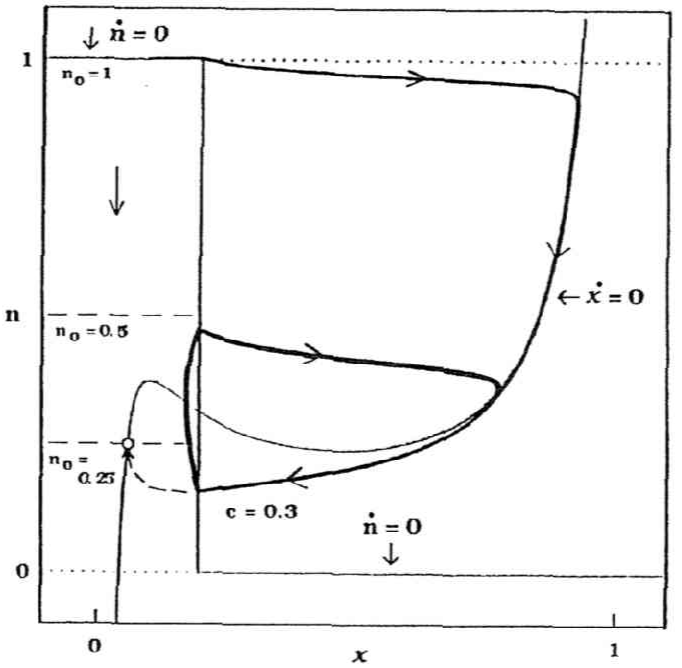

Fig. 10

Appendix I

The FitzHugh (or BVP) model

$$\dot{x} = x - \frac{x^3}{3} - y + I$$

$$\dot{y} = \phi(x + a - by)$$

a, b, and ϕ: positive constants
x: the membrane potential
y: the recovery valuable
I: the membrane current

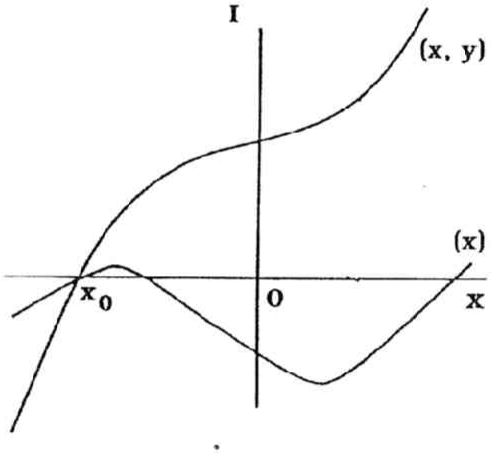

The Murase model

$$\gamma \dot{x} = Anx^2(1 - x) - K_e x + Z$$

$$\dot{n} = \begin{cases} b(1 - n) & (x \le x_a) \\ - cn & (x > x_a) \end{cases}$$

A, b, c, K_e, x_a and γ: positive constants
x: the shear displacement
n: the fraction of attached cross-bridges
Z: the external shear force

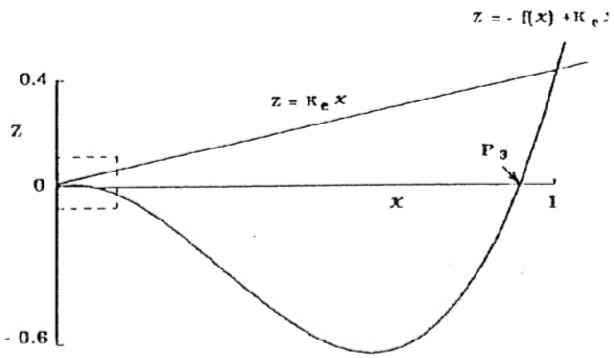

Appendix II

The FitzHugh (or BVP) model

$$\dot{x} = 0 \qquad y = x - \frac{x^3}{3} + I$$

$$\dot{y} = 0 \qquad y = \frac{x + a}{b}$$

a, and b: positive constants
x: the membrane potential
y: the recovery valuable
I: the membrane current

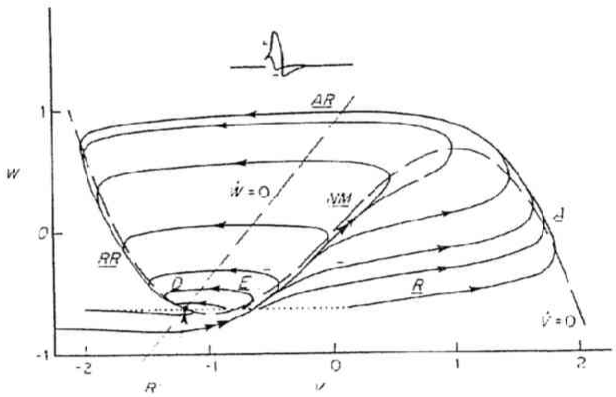

The Murase model

$$\dot{x} = 0 \qquad n = \frac{K_e x - Z}{Ax^2(1 - x)}$$

$$\dot{n} = 0 \qquad n = \begin{cases} 1 & (x \le x_a) \\ 0 & (x > x_a) \end{cases}$$

A, b, c, K_e, and x_a: positive constants
x: the shear displacement
n: the fraction of attached cross-bridges
Z: the external shear force